Supplementary Information (SI) for Chemical Science.

Supporting Information

Phase Effect of TiO_2 on Surface Hydrogen Adsorption/Desorption in Controlling Photocatalytic Methane Conversion

Jiakang You[1], Ardeshir Baktash[1], Dazhi Yao[2], Yanzhao Zhang[1], Shanshan Ding[1], Jingwei Hou[1], Guangyu Zhao[2], Yonggang Jin[2], Zhiliang Wang[1*], Lianzhou Wang[1*]

[1]Nanomaterials Centre, School of Chemical Engineering and Australian Institute for Bioengineering and Nanotechnology, The University of Queensland, St Lucia, Queensland, 4072, Australia.

[2]CSIRO Mineral Resources, 1 Technology Court, Pullenvale, QLD 4069, Australia

Email: zhiliang.wang@uq.edu.au; l.wang@uq.edu.au

Methods

Chemicals

TiO_2 (Sigma-Aldrich 637254, Anatase nanopowder, <25 nm particle size, ≥99.7% trace metals basis), TiO_2 (Sigma-Aldrich 637262, Rutile nanopowder, <100 nm particle size, ≥99.5% trace metals basis), $HAuCl_4 \cdot 3H_2O$ (Sigma-Aldrich, ACS reagent, ≥49.0% Au basis), and Methanol (were used without further purification. Deionised (DI) water was used throughout the experiment.

Preparation of TiO_2 photocatalysts containing different ratio of anatase and rutile phases

TiO_2 photocatalysts with different ratio of anatase and rutile phases were prepared through a simple thermal treatment method. One-gram commercial anatase powder was calcinated at different temperatures (700, 800, 850, 900, and 1000 °C) in a muffle furnace for 2 hours at a heating rate of 5 °C/min. Finally, TiO_2 photocatalysts with different ratio of anatase and rutile phases were obtained, named as T-700, T-800, T-850, T-900, and T-1000, respectively. Commercial rutile TiO_2 nanoparticles obtained from Sigma-Aldrich were used as a reference. The same heating procedure was used with the commercial rutile TiO_2 nanoparticles as the starting materials to get treated samples, named as R-700, R-800, R-900, and R-1000.

Photodeposition of Au nanoparticles

Ten-milligram TiO_2 powder and a calculated amount of gold precursors (5 wt%, $HAuCl_4$) were mixed in an aqueous solution (4 mL DI water and 1 mL methanol as electron donor). The suspension was then irradiated by a 300 W Xe lamp under vigorous stirring. After one-hour photodeposition, the suspension was washed with water three times, filtered on a glass fiber membrane, and finally dried in an oven at 60 °C overnight.

Characterization

X-ray photoelectron spectroscopy (XPS) with an Al Kα X-ray radiation source was used to characterise the surface carbon content of the material. Transmission electron microscopy (TEM) imaging was carried out using Hitachi HT 7700 120 kV TEM. High-resolution TEM imaging was carried out using Hitachi HF5000 Cs-STEM/TEM 200 kV. Scanning electron microscopy (SEM) imaging was carried using JEOL JSM-7100F. The UV-vis absorption spectra were obtained using a JASCO V-650 spectrophotometer. Raman spectroscopy was carried out using a confocal Raman microscope (RM5, Edinburgh Instruments) with a 10X objective and a 532 nm laser in all experiments. The crystalline phase of the samples was characterised by synchrotron X-ray powder diffraction with a Mythen-II detector on the powder diffraction beamline at the Australian Synchrotron with a wavelength (λ) of 0.6888 Å. The ratio of anatase phase and rutile phase in TiO_2 photocatalysts is evaluated by the following equations[1]:

$$Ratio\ of\ anatase = \frac{K_a I_A}{K_a I_A + I_R} \times 100\% \qquad \text{S1}$$

$$Ratio\ of\ rutile = \frac{I_R}{K_a I_A + I_R} \times 100\% \qquad \text{S2}$$

Where I_A and I_R represent the integrated area of $(101)_{\mathrm{Anatase}}$ and $(110)_{\mathrm{Rutile}}$ peaks, respectively. K_a stands for a correction coefficient, i.e., 0.886.[2]

The light absorption ability of the solid powder samples was quantified by UV-vis spectra using the following equation reported in literature[3, 4]:

$$\mathrm{LHE} = 1 - 10^{-A_{(\lambda)}} \qquad \text{S3}$$

Wherein $A_{(\lambda)}$ is the absorbance at wavelength λ, LHE is the light harvest efficiency.

The time-resolved photoluminescence (TRPL) decay studies were carried out with a 377 nm pulsed diode laser excitation source on a fluorescence spectrophotometer (FLSP-900, Edinburgh Instruments). The average carrier recombination lifetime (τ_{average}) of the TiO_2 photocatalysts was calculated by fitting the TRPL decay curves with a bi-exponential function of time (t)[5]:

$$F(t) = A_1 e^{-\frac{t}{\tau_1}} + A_2 e^{-\frac{t}{\tau_2}} + y_0 \qquad \text{S4}$$

$$\tau_{average} = \frac{A_1\tau_1^2 + A_2\tau_2^2}{A_1\tau_1 + A_2\tau_2} \qquad \text{S5}$$

where τ_1 and τ_2 are the time constants of the fast (i.e., surface recombination) and slow (i.e., bulk recombination) decay process, respectively. A_1, A_2, and y_0 are constants.[6, 7]

Temperature programmed desorption mass spectrometry of methane (CH_4-TPD-MS) was conducted on a BELCAT II Analyser equipped with a mass spectrometer (MS). Prior to the CH4-TPD analysis, 60 mg of sample was placed in a quartz reactor located in a furnace and purged with Ar (40 ml/min) at 150 °C for 1 h. The pre-adsorption process was carried out with a stream of 5 vol% CH_4 in Ar (40 ml/min) at 150 °C for 30 min, followed by cooling to 60 °C in pure Ar. The adsorbed CH_4 was then removed by passing Ar (40 ml/min) in a temperature range of 60 - 800 °C with a ramp rate of 5 °C/min. The desorbed gases were monitored using the MS detector.

In-situ electron paramagnetic resonance (EPR) spectra were collected on a Bruker Elexsys E500 spectrometer equipped with an ElexSys Super High Sensitivity Probehead and liquid nitrogen cooling using a cryogen-free cryostat (Bruker waveguide Cryogen-free system with recirculatory, WVGD SYS 5K F70H wRCRC 2). The magnetic field was calibrated with a Gauss meter and measurements were conducted using a modulation amplitude of 0.8 mT, a modulation frequency of 100 kHz and a microwave power of 5 mW (10 dB of 200 mW, non-saturating condition).

The specific surface area of each sample was determined by the nitrogen adsorption-desorption isotherms measured at 77 K (Micrometrics Instrument Corporation, Tristar nitrogen sorption instrument). The specific surface area (SSA) was derived by using the following equation.[8]

$$SSA = \frac{V_m \cdot N_A \cdot a_m}{v_m \cdot m_s}$$

where V_m is the monolayer volume, N_A is the Avogadro's number, a_m is the effective cross-section area of one adsorbed molecule, v_m is the molar volume of one adsorbed molecule, and m_s is the mass of the sample.

Photocatalytic oxidative coupling of methane (POCM) performance measurement

POCM reaction was conducted in a 50 mL flow reactor made of stainless steel (PLR-GPTR 50, Perfectlight Technology Co., Ltd). Ultra-high purity CH_4 gas (>99.995%) was used in this experiment. Typically, the aforementioned glass fiber membrane loaded with TiO_2 photocatalysts was put into the reactor covered by an optical quartz window. Reaction gas with a total flowrate of 126 mL min-1 (gas ratio CH_4/O_2, 125/1) was introduced to the reactor. The reactor was illuminated by a 300 W Xe lamp (full spectrum, Perfectlight Technology Co., Ltd). The gas products were quantitatively analyzed by gas chromatography (GC-2014, Shimadzu).

For the measurement of the apparent quantum yield (AQY), the same procedure of POCM performance measurement was followed using the same lamp but equipped with a 350 nm bandpass filter as the light source.

The AQY was calculated according to the following equation:

$$AQY = \frac{N(electrons)}{N(photons)} \times 100\% \qquad \text{S6}$$

where N(electrons) and N(photons) represent the number of reacted electrons and the number of incident photons, respectively. According to the chemical equation ($2CH_4+1/2O_2 \rightarrow C_2H_6+H_2O$; $8CH_4+3O_2 \rightarrow CO_2+4H_2O$), the reacted electrons for each product can be calculated according to the following equation:

$$N(electrons) = 2 \times N(C_2H_6) + 8 \times N(CO_2) \qquad \text{S7a}$$

$$= 2 \times M(C_2H_6)N_A + 8 \times M(CO_2)N_A \qquad \text{S7b}$$

where N(product), M(product) and N_A represent the number of produced molecules for the specific product, the number of moles of the products and Avogadro's constant, respectively.

The number of incident photons was calculated according to the following equation:

$$N(photons) = \frac{I \times A \times \lambda}{hc \times EQE(Si)} \qquad \text{S8}$$

where, I is the light intensity measured by photodetector (W cm^{-2}); A is the irradiation area, λ is the wavelength of the incident light, h is Planck constant, c is the speed of light, EQE(Si) is the external quantum efficiency of the detector at certain wavelength.

Photocurrent measurement

The photoelectrode was prepared by using a drop casting method. The drop casting ink was prepared by dispersing 3 mg of catalyst in 490 uL deionized water and 490 uL ethanol, and 20 uL 5% Nafion 117 solution was added as a binder. Then, the ink was sonicated for 30 minutes in an ice bath to generate a uniform ink. After that, the ink was dropped on a piece of FTO glass. The photoelectrode will be ready to use after drying in an oven at 60 °C overnight.

All the photocurrent measurements were carried out in a three-electrode system with Pt foil as counter electrode and silver/silver chloride electrode as a reference electrode. The Xenon lamp (Perfectlight) equipped with AM 1.5 G filter was applied as the light source with a light intensity of 100 mW cm^{-2}.

Computational method

In this study, Vienna Ab Initio Simulation Package (VASP) package is used for all the density functional theory (DFT).[9] The generalized gradient approximation (GGA) method, employing the Perdew-Burke-Ernzerhof (PBE) functional with a D3-BJ dispersion correction, was used to describe exchange-correlation effects in all calculations.[10-12] The projector augmented-wave (PAW) method with an energy cutoff of 520 eV and a force tolerance of 0.01 eV/Å is used to describe the core and valence electrons for ground state energy optimizations. Here a supercell of 96 and 108 atoms are considered to model the anatase (101) and (110) rutile TiO_2 surfaces. To model surfaces, bulk structures were initially optimized. These optimized structures served as the basis for subsequent surface modelling. For ground state geometry optimization of anatase and rutile surfaces, the bottom layer was fixed, while atoms in higher layers were allowed to relax freely to achieve convergence. To model surfaces, bulk structures were optimized. These optimized structures were then used to create surface models. For ground state geometry optimization of anatase and rutile surface structures, the bottom layer was fixed, imposing a constrained condition on these atoms. Atoms in higher layers were allowed to relax until convergence was reached. To minimize the influence of periodic boundary conditions, a vacuum layer of 18 Å was applied to anatase structures, while a 20 Å vacuum was used for rutile structures. Vibrational frequency calculations were performed to determine the Gibbs free energies of the structures with adsorbents.

Supplementary Figures

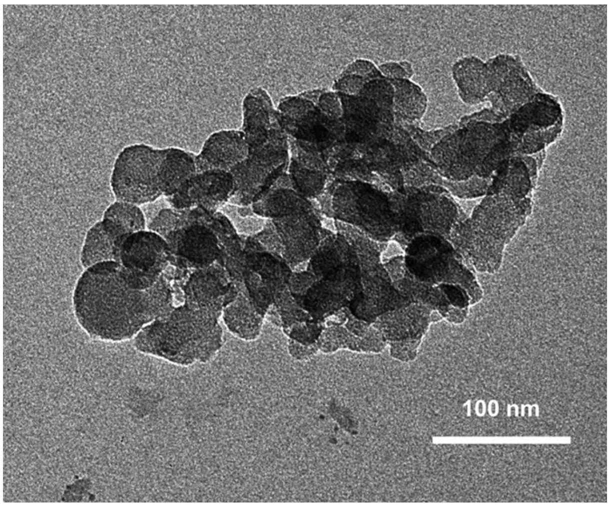

Figure S1 TEM image of anatase TiO_2 nanoparticles purchased from Sigma-Aldrich.

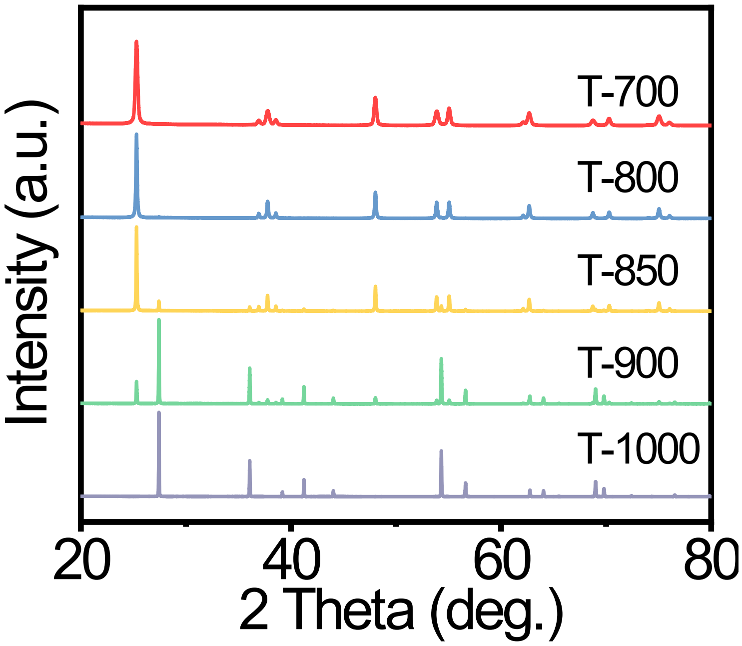

Figure S2 Synchrotron-based powder diffraction patterns of as-prepared TiO_2 photocatalysts calcined at different temperatures, e.g. T-700 was calcined at 700°C.

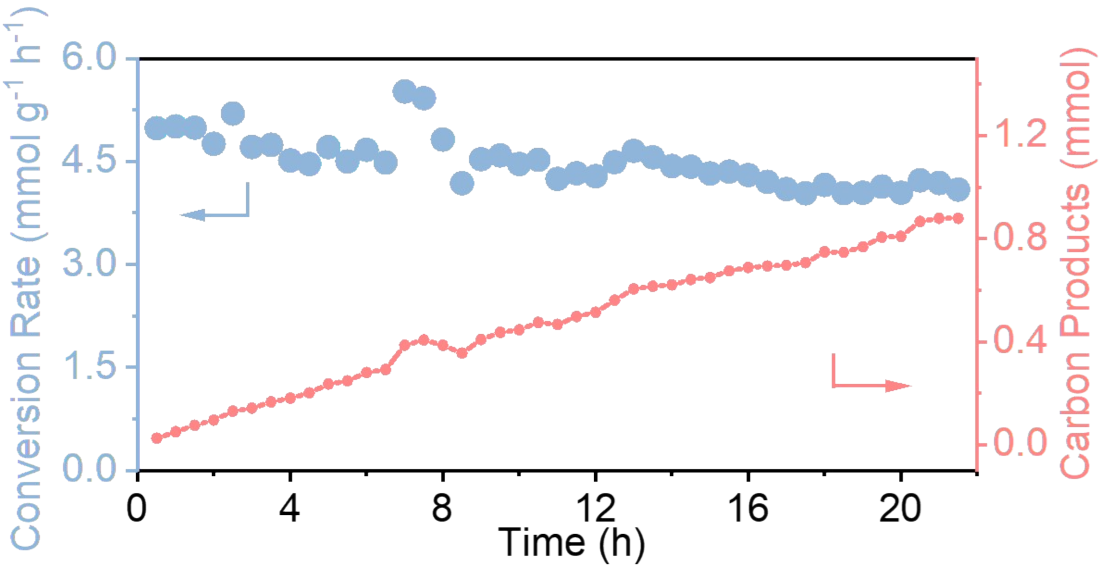

Figure S3 Stability test of the POCM over Au loaded T-700 sample in a flow reactor. The CH_4 conversion rate and total conversion amount have been monitored

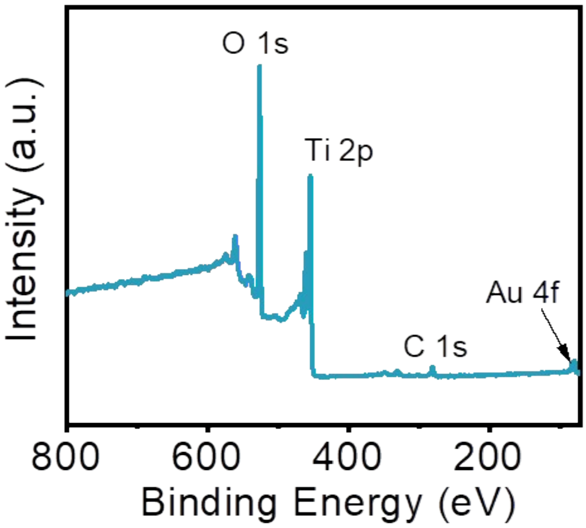

Figure S4 XPS survey scan of Au loaded T-700 sample.

The surface carbon content of the T-700 sample is estimated to be around 4.7 wt %. Given that 10 mg of photocatalyst was used for the tests, the estimated surface carbon content was approximately 0.04 mmol. Based on our long-term stability test, the total amount of carbon products produced was calculated to be approximately 0.8 mmol (Figure S3), with no significant decline in performance. Therefore, we can safely rule out the potential influence of carbon contamination on the POCM process. Herein, we have calculated the utmost carbon contamination from the carbon C 1s peak since ubiquitous carbon contamination from atmosphere exposure or the volatilization of organic molecules from XPS sample containers is very common and generally been adopted as internal calibration. Therefore, the actual carbon contamination is expected to be lower than the content detected by XPS.

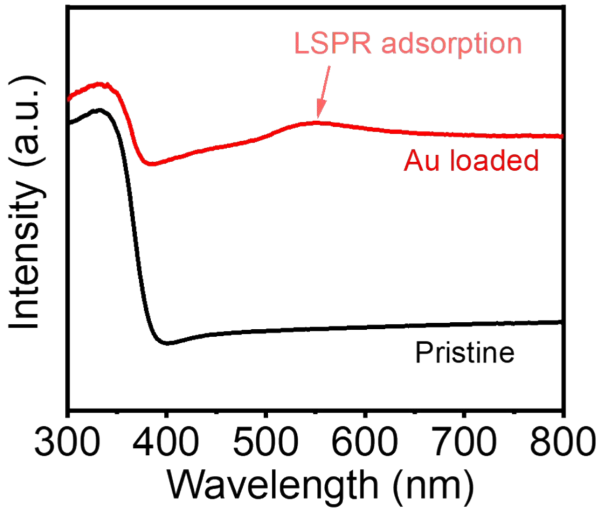

Figure S5 UV-vis spectra of the Au-loaded and pristine anatase photocatalysts.

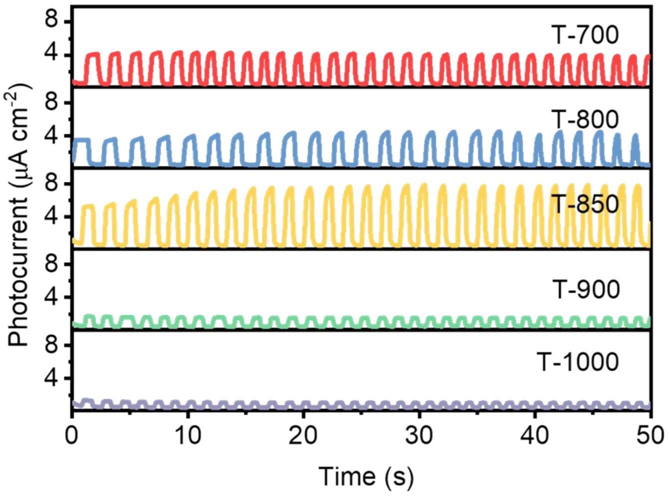

Figure S6 Photocurrent measurement at 1.23 V vs RHE in 1M Na_2SO_4 solution over as-prepared TiO_2 photocatalysts. Light source: Xe lamp (100 mW cm^{-2}) with AM 1.5 G filter.

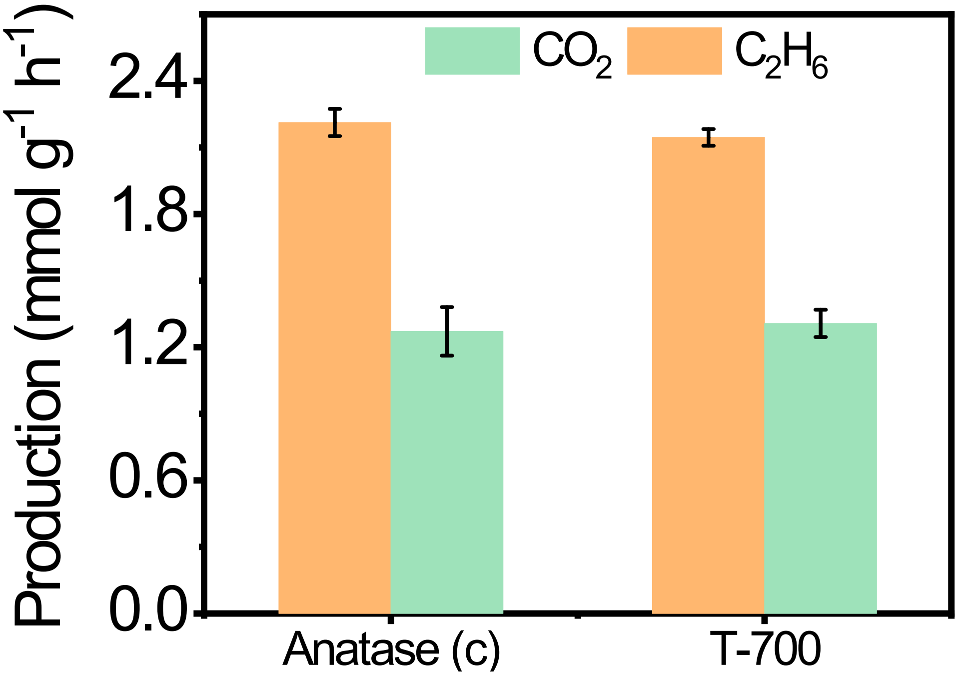

Figure S7 POCM performance of commercial anatase and T-700 treated sample.

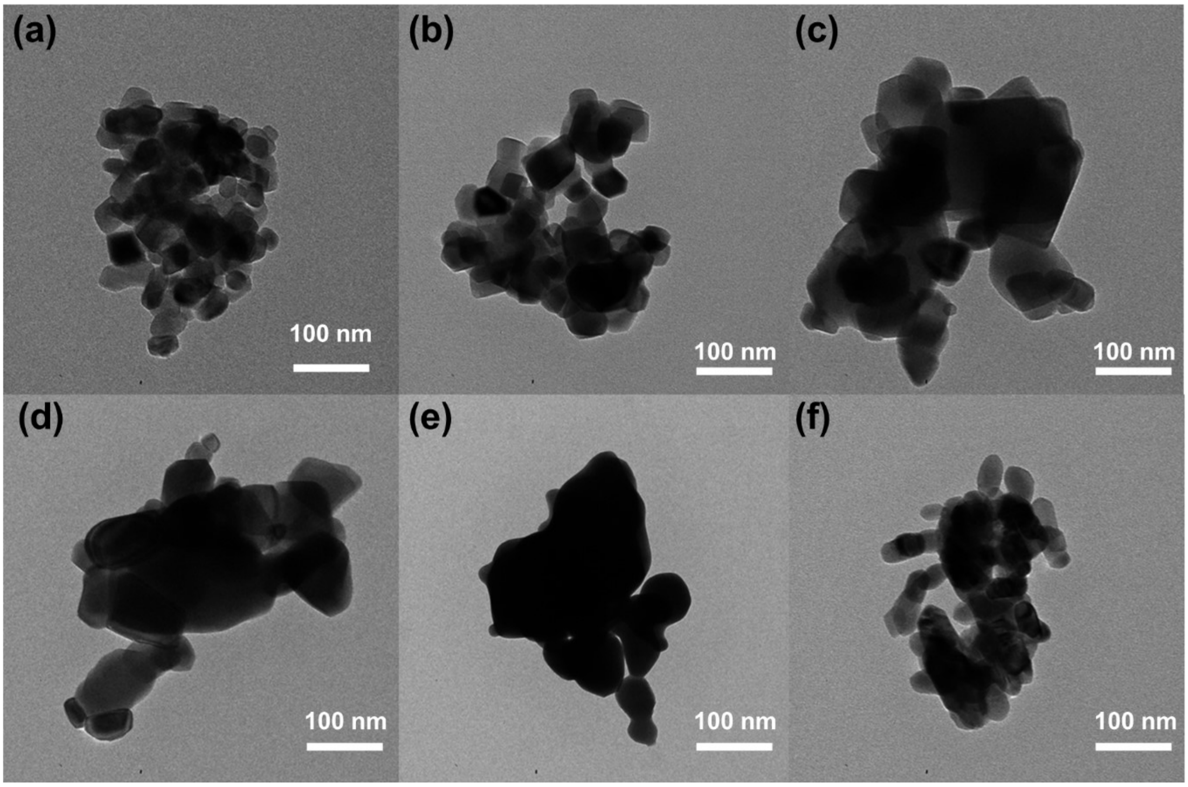

Figure S8 TEM images of T-700 (a), T-800 (b), T-850 (c), T-900 (d), T-1000 (e), and commercial rutile TiO_2 nanoparticles (f).

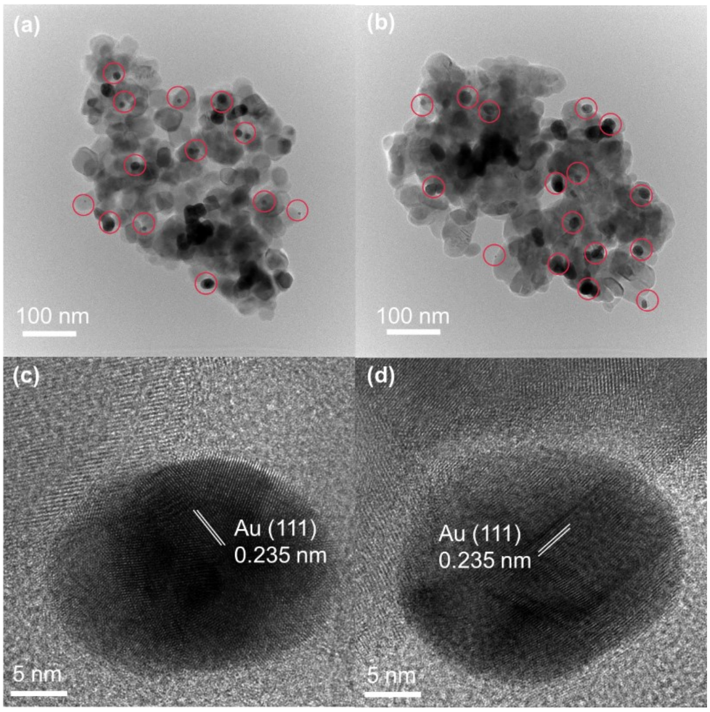

Figure S9 TEM and HRTEM images of Au loaded T-700 (a) and (c) and Au loaded commercial rutile TiO_2 nanoparticles (b) and (d). Red circles on (a) and (b) are Au nanoparticles. Comparing the anatase with the rutile nanoparticles, they show similar particle size of both TiO_2 and loaded gold nanoparticles. The Au-TiO_2 interface in (c) and (d) also indicates their interfaces are in similar status.

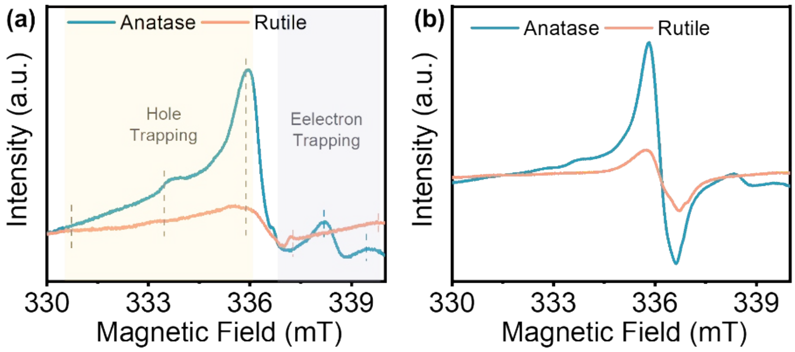

Figure S10 In-situ EPR spectra of anatase and rutile under light (a) without CH_4 and (b) with CH_4.

Table S1 Ratio of anatase phase and rutile phase in as-prepared TiO_2 photocatalysts based on synchrotron-based powder diffraction patterns.

Sample Name	**I_A**	**I_R**	**K_a**	**Ratio of anatase phase**	**Ratio of rutile phase**
T-700	0.29	0	0.886	100.00%	0.00%
T-800	0.17	0.001	0.886	99.42%	0.58%
T-850	0.11	0.009	0.886	91.28%	8.72%
T-900	0.02	0.073	0.886	22.84%	77.16%
T-1000	0	0.062	0.886	0.00%	100.00%

Table S2 Fitted parameters of the TRPL curves of TiO_2 photocatalysts.

Sample Name	**A_1**	**A_2**	**τ_1 (ns)**	**τ_2 (ns)**	**$\tau_{average}$ (ns)**
T-700	1270.54	18.49	1.06	6.7	1.54
T-800	880.55	149.4	1.1	8.78	5.52
T-850	793.03	225.94	1.16	10.23	7.65
T-900	731.9	124.71	1.5	10.32	6.26
T-1000	771.49	180.46	1.22	6.95	4.49

Table S3 Pearson Correlation Coefficient (PCC) analysis between CH_4 conversion and different parameters.

CH_4 Conversion Rate (mmol g^{-1} h^{-1})	**5.60**	**3.95**	**2.90**	**0.38**	**0**	**PCC**
Anatase ratio	100.00%	99.42%	91.28%	22.84%	0.00%	0.93
Anatase surface area (m^2 g^{-1})	42.01	17.64	7.24	0.88	0	0.92
Charge carrier lifetime (ns)	1.54	5.52	7.65	6.26	4.49	-0.47
Light Absorbance (%)	2.65%	2.68%	3.25%	3.59%	4.00%	-0.95

Table S4 Specific surface areas of TiO_2 photocatalysts based on Brunauer-Emmett-Teller (BET) analysis.

Starting materials	Surface area (m^2 g^{-1})	Treated Samples	Surface area (m^2 g^{-1})
Anatase (Sigma-Aldrich, batch NO. 637254)	77	T-700	42
		T-800	18
		T-850	8
		T-900	4
		T-1000	2
Rutile (Sigma-Aldrich, batch NO. 637262)	32	R-700	18
		R-800	14
		R-900	5
		R-1000	1

References

1. R. A. Spurr and H. Myers, *Anal. Chem.*, 1957, **29**, 760-762.
2. Y. Jiang, W. Zhao, S. Li, S. Wang, Y. Fan, F. Wang, X. Qiu, Y. Zhu, Y. Zhang, C. Long and Z. Tang, *J. Am. Chem. Soc.*, 2022, **144**, 15977-15987.
3. Z. Wang, Y. Qi, C. Ding, D. Fan, G. Liu, Y. Zhao and C. Li, *Chem. Sci.*, 2016, **7**, 4391-4399.
4. T. W. Kim and K.-S. Choi, *Science*, 2014, **343**, 990-994.
5. M. Hao, Y. Bai, S. Zeiske, L. Ren, J. Liu, Y. Yuan, N. Zarrabi, N. Cheng, M. Ghasemi, P. Chen, M. Lyu, D. He, J.-H. Yun, Y. Du, Y. Wang, S. Ding, A. Armin, P. Meredith, G. Liu, H.-M. Cheng and L. Wang, *Nat. Energy*, 2020, **5**, 79-88.
6. P. Chen, Y. Bai, S. Wang, M. Lyu, J.-H. Yun and L. Wang, *Adv. Funct. Mater.*, 2018, **28**, 1706923.
7. S. Ding, J. A. Steele, P. Chen, T. Lin, D. He, C. Zhang, X. Fan, E. Solano, A. K. Whittaker, M. Hao and L. Wang, *Adv. Energy Mater.*, 2023, **13**, 2301817.
8. M. Naderi, in *Progress in Filtration and Separation*, ed. S. Tarleton, Academic Press, Oxford, 2015, 585-608.
9. G. Kresse and J. Furthmüller, *Phys. Rev. B*, 1996, **54**, 11169-11186.
10. J. P. Perdew, K. Burke and M. Ernzerhof, *Phys. Rev. Lett.*, 1996, **77**, 3865-3868.

11. S. Grimme, J. Antony, S. Ehrlich and H. Krieg, *J. Chem. Phys.*, 2010, **132**.

12. S. Grimme, S. Ehrlich and L. Goerigk, *J. Comput. Chem.*, 2011, **32**, 1456-1465.